

# MONTE-CARLO RE-DEPOSITION MODEL DURING TERRESTRIAL MEASUREMENTS OF ION THRUSTERS

JULIA DURAS<sup>a,\*</sup>, OLEKSANDER KALENTEV<sup>a</sup>, RALF SCHNEIDER<sup>a,b</sup>,  
KONSTANTIN MATYASH<sup>b</sup>, KARL FELIX LÜSKOW<sup>a</sup>, JÜRGEN GEISER<sup>a</sup>

<sup>a</sup> *Institute of Physics, Ernst-Moritz-Arndt University Greifswald, Felix-Hausdorff-Str.6, D-17498 Greifswald, Germany*

<sup>b</sup> *Computing Center, Ernst-Moritz-Arndt University Greifswald, Felix-Hausdorff-Str.12, D-17498 Greifswald, Germany*

\* corresponding author: [julia.duras@physik.uni-greifswald.de](mailto:julia.duras@physik.uni-greifswald.de)

**ABSTRACT.** For satellite missions, thrusters have to be qualified in large vacuum vessels to simulate the space environment. One caveat of these experiments is the possible modification of the beam properties due to the interaction of the energetic ions with the vessel walls. Impinging ions can produce sputtered impurities or secondary electrons from the wall. These can stream back into the acceleration channel of the thruster and produce co-deposited layers. Over a long operation time of thousands of hours, these layers can modify the optimized geometry and induce changes in the ion beam properties, e.g., broadening of the angular distribution and thrust reduction. A Monte Carlo code for simulating the interaction of ion thruster beams with vessel walls was developed to study these effects. Back-fluxes of a SPT-like ion thruster for two different test-setups and vessel geometries are calculated.

**KEYWORDS:** Ion thruster, Monte-Carlo method, terrestrial testing of thrusters, interaction with vessel walls.

## 1. INTRODUCTION

Ion thrusters, where the propellant is ionized and the ions are accelerated by electric fields, are of increasing importance for scientific and commercial space missions. Compared to commonly used chemical thrusters they have a 5 to 10 times higher specific impulse [1]. This results in a considerably reduced propellant budget, and a significant reduction of spacecraft launch mass by some 100 to 1000 kg can be achieved. One concept for this electric propulsion involves grid-less ion thrusters, which are based on magnetic confinement of the plasma electrons, where the trapped electrons both ionize the propellant and provide the potential drop for ion acceleration. Due to their low complexity in terms of system architecture, they are becoming of increasing interest in particular for commercial satellites.

In order to reduce the development and qualification costs, it is therefore necessary to set up and apply a series of different modeling tools which can quantitatively describe the plasma physics within the thruster, and also the interactions of the thruster with the testing environment and finally with the satellite. The integrated modeling strategy should include several modular components in a consistent way in order to provide the complexity and accuracy required for the problem [2].

Ions created in the thruster discharge may impinge on the surrounding surfaces, which can induce sputter erosion and redeposition of eroded material. Depending on the surface region, this may affect the opera-

tional and performance characteristics of the thruster itself, of the ion thruster module, or even of the whole satellite. For the simulation, one can distinguish:

- (a) The impact on the inner thruster surface by ions generated in the inner thruster discharge.
- (b) The impact on the exit-sided surface of the thruster and the neutralizing electron source by ions generated in the plasma plume downstream the thruster exit.
- (c) The impact on the satellite surface producing erosion and redeposition.
- (d) The impact on the vacuum chamber walls during testing and life-time qualification, creating redeposition onto the thruster and thruster module surface.

The proposed multi-scale modeling strategy is well suited to address these ion impingement effects.

The outline of the paper is as follows: the modeling strategy is described and the problems of artifacts during terrestrial qualifications are outlined. As one example of this modeling, the influence of the test-setups on particle back-fluxes towards the ion thruster channel is studied with a Monte Carlo model for an SPT-like ion thruster. Finally, the results are summarized.

## 2. MODELING STRATEGY

The most complete model resolving all time scales of ion thrusters would be a direct coupling of a kinetic plasma model with a molecular dynamics model for the walls. This would allow a fully self-consistent

analysis of the complete system, including plasma dynamics, possible erosion of the thruster walls and the interaction of the exhausted ions with the surrounding satellite surfaces or, during testing and qualification, with the testing environment, like the vacuum chamber walls. This type of solution is not feasible, due to the tremendous computational costs and the high complexity of this combined model. Instead, we propose to use a hierarchical multi-scale set of models, in which the parameterization for a lower hierarchy model can be deduced from a higher level model.

For example, a 3D particle-in-cell (PIC) model can deliver a parameterization of turbulence effects by appropriate anomalous transport coefficients. Transport coefficients based on these runs could then be used in a 2D PIC, which is more practical for production runs.

To get a correct description of both the thruster and the plume plasma, one has to solve a kinetic problem for the whole region of interest, including all significant physical processes. These are collisions, turbulence effects, surface driven sheath instabilities and breathing modes. A PIC model is therefore a natural choice for this problem. In addition, similarity scaling is applied to further reduce the calculation costs [3].

In order to describe erosion-redeposition processes, one can use various approximation levels of the model. The most thorough description is given by the full molecular dynamic model. However, this would be far too time-consuming, because it resolves each individual atom and their interactions. The next level can be represented by the binary collision cascade model, which assumes an amorphous target and the interaction of particles with the solid based on heavy particle collisions with ions, and additional losses with electrons acting as a viscous force. This model can use the detailed information about flux distributions provided by the PIC code, and can then, on the basis of this, the erosion response of the materials. The most crude approximation is given by a Monte-Carlo (MC) procedure simulating erosion-redeposition on the basis of sputter yield tables calculated from the binary-collision cascade or molecular dynamics model together with information about the plasma fluxes. This model is particularly useful due to its simplicity and flexibility for the quantifying the lifetime of ion thrusters.

### 3. ARTIFACTS DURING TERRESTRIAL MEASUREMENTS OF AN ION THRUSTER

Terrestrial qualification of a thruster differs significantly from outer space exploitation, in that it is held in a limited vessel, which can create various artifacts on the measured thruster properties. For example, the back scattered flux from the vessel walls can be

deposited on the walls of the thrusters, and can in that way form a conducting layer influencing the thruster operating regimes. These measurements are taken in large vacuum vessels, up to 10 times larger than the thruster itself, in order to provide a space-like environment. Despite these dimensions, however interactions of exhausted particles with residual gas and vessel walls still take place and can modify the measurements. One source of differences between measurements in space and during terrestrial testing is the re-deposition of sputtered particles inside the thruster channel or for the grid thruster at the thruster walls. The accelerated ions impinge on the vessel walls and produce sputtered impurities. These can stream back towards the acceleration channel of the thruster and produce co-deposited layers. Over a long operation time of thousands of hours, these layers can modify the optimized geometry of the thruster channel or grids and the inner wall surface. This induces changes in the ion beam properties, e.g., broadening of the angular distribution and thrust reduction, as observed in the test campaigns of HEMP-T [4] and the NEXT grid thruster [5]. A reduced back-flux is therefore important to minimize artifacts in the plume measurements.

Due to the large size difference between the thruster and the vessel, it is possible to parameterize the back-scattered flux from the vessel walls as an effective source for the MC erosion-deposition code. This paper will show that the position of the thruster inside the vessel, the wall material and the vessel geometry play important roles and can influence the plume measurement results.

### 4. DESCRIPTION OF THE MONTE CARLO MODEL

The Monte Carlo (MC) method is a common approach for plasma-wall problems, for example MC simulations of sputtering and re-deposition are well established in fusion-oriented studies [6] as is magnetron sputtering [7, 8]. The idea of the Monte Carlo model is to sample the primary distribution of the ions with respect to energies, angles and species. These pseudo-particles are followed hitting the vessel walls and generating sputtered particles, based on sputter rates calculated by a binary collision cascade code. Their angular distributions are sampled and the back-flow of the eroded particles from the vessel walls towards the ion thruster acceleration channel is calculated.

In this work, we assume that particles move along rays according to their source distribution. In this 3D model, the vacuum chamber is assumed to be a cylinder with two spherical caps attached to its ends. The angular source distributions of the mean ion energy, the current and the species fraction were generated with respect to the emission angle  $\theta$ , see Fig. 3. As an example, ion current and energy distributions similar to those published for SPT-100 [9] are used. The fraction of  $\text{Xe}^{2+}$  to  $\text{Xe}^+$  ions is taken

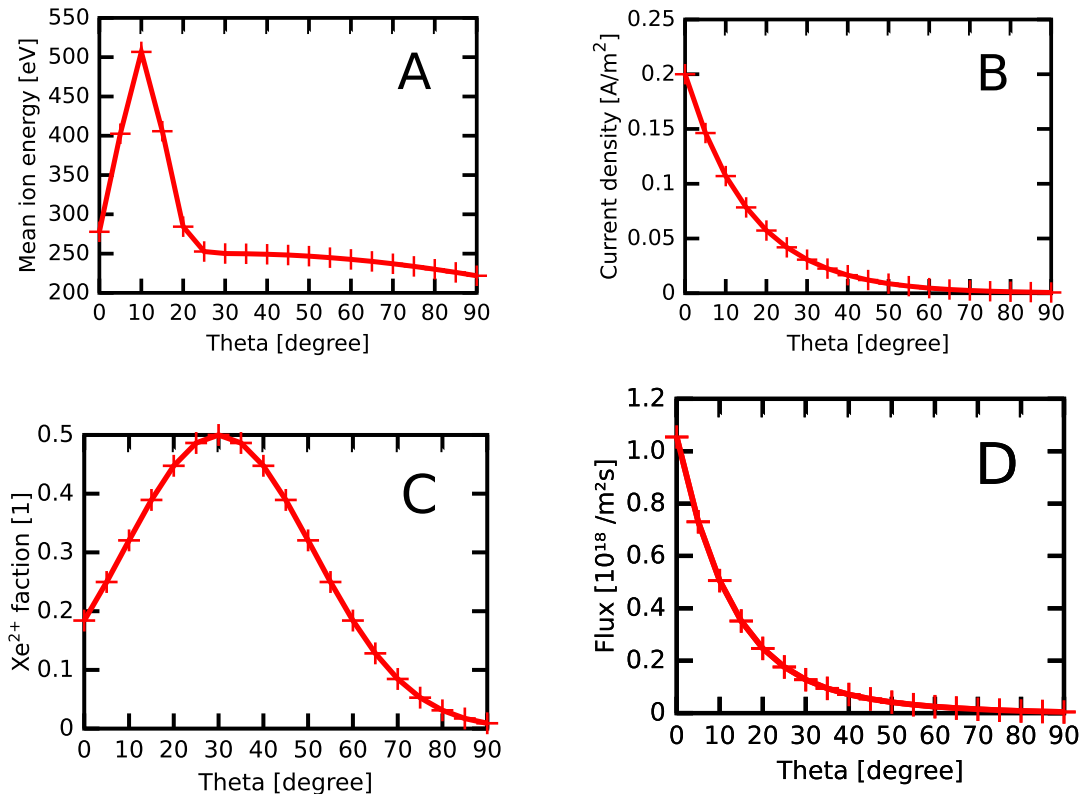


FIGURE 1. Distribution of mean ion energy (A), current density (B), Xe<sup>2+</sup> fraction (C) and the resulting emitted flux (D) similar to SPT-100.

arbitrarily. All used source distributions used here are shown in Fig. 1(A)–(C), sampled as a point source at the thruster exit, within angular steps of  $\Delta\theta = 5^\circ$ . The resulting emitted flux

$$\Gamma(\theta) = \frac{j(\theta)}{e \cdot (1 + f^{\text{em}}(\theta))}$$

is shown in Fig. 1(D), where  $j(\theta)$  is the current density,  $e$  is the elementary charge and  $f^{\text{em}}(\theta)$  is the emitted Xe<sup>2+</sup> fraction. Equal distribution of the poloidal angle is used. This distribution represents an emitted beam of Xenon ions with a mean emission angle of  $\theta^{\text{em}} = 0^\circ$ . The sputter yield for the impinging ions on the vessel walls is taken from SDTrimSP [10] simulations. While the thruster is operating, ions with energies larger than the sputter threshold form a micro roughness on the thruster surfaces. Due to shadowing, this micro-roughness modifies the real angle of incidence, effectively reducing its range to values between 20° and 50°. For this angular range, the sputter yields vary only slightly with angle. We therefore assume that the sputter yields depend only on the energy of the impinging ions. It is also assumed that the sputtered particles obey a cosine law [11] for their angular distribution. Due to their low energies, the sputtered particles are assumed to have a sticking coefficient of 1. Therefore, only particles with direction towards the thruster exit are followed. A detailed description of the Monte Carlo model and its validation with analytic calculations can be found in [12].

In the following, the influence of the thruster position inside the vessel is studied. This is important, since ion thrusters are qualified within various test-setups.

## 5. BACK-FLUX FOR TWO DIFFERENT TEST-SETUPS

Measurements of plume parameters are taken in two different test-setups: a 'performance test', where a single thruster is placed in the center of the circular cross-section of the vessel, and an 'end-to-end test', where four thrusters are assembled as a cluster. Performance tests are typically carried out to test and qualifying single thrusters, while end-to-end tests give the characteristics of a whole cluster of thrusters, as it is applied on satellites where only one of the thrusters is operating. The following comparison of the two test setups shows strong dependency of the back-flux on this thruster position.

For the performance test, the ion thruster is placed co-axially in the vessel. In the following, the LVTF-1 vessel at Aerospazio [13] in Siena, Italy was taken as a reference. It has a cylinder length of  $Z_c = 7.7$  m and a radius of  $R_c = 1.9$  m. The spherical cap at the end has a radius of  $R_{sp} = 2.7$  m. For simplicity, the ion thruster is approximated by a cylinder with a length of  $L = 9.0$  cm and a diameter of  $D = 9.0$  cm. In most test chambers, graphite-coated walls are used in order to reduce the back-fluxes of sputtered par-

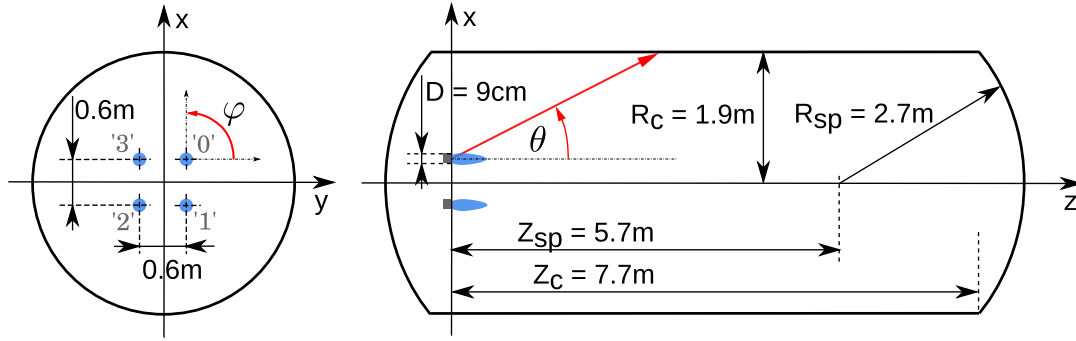


FIGURE 3. Sketch of a thruster cluster assembled in the LVTF-1 vessel within an end-to-end test set-up. ‘0’ to ‘3’ indicate the different thrusters.

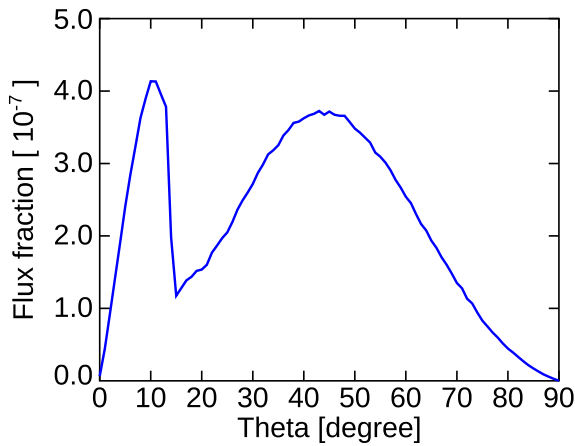


FIGURE 2. Calculated back-flux towards the thruster exit in total (total flux fraction of  $1.97 \cdot 10^{-5}$ ).

ticles, since graphite has a lower sputter yield than aluminum. However, in the case of carbon the release of hydrocarbons is a major problem linked to the sponge-like characteristics of carbon with respect to its interaction with hydrogen. The sputtered hydrocarbons produce a co-deposited layer inside the thruster channel, which can become conductive and can therefore change the potentials and can produce subsequent problems. When carbon is replaced by metal walls, the rates of physical sputtering are larger, but the evaporation in the hot parts of the channel will prevent deposition inside the thruster [2]. Aluminum walls are therefore studied with the Monte-Carlo model.

Within this model, the back-flux is collected on a circle, which represents the thruster exit. The calculated back-flux fraction towards the source is shown by a blue line in Fig. 2. It is given by the number of particles hitting the thruster exit in a certain angular range  $[\theta; \theta + \Delta\theta]$ , with  $\Delta\theta = 1^\circ$ , divided by the total number of source particles. For the chosen parameters of the vessel, the back-flux for  $\theta = [0; 14^\circ]$  originates from the spherical cap, while for  $\theta = [14^\circ; 90^\circ]$  it comes from the cylindrical walls of the vessel. The flux fraction shows a pronounced peak at around  $10^\circ$  and a broader peak at about  $45^\circ$ .

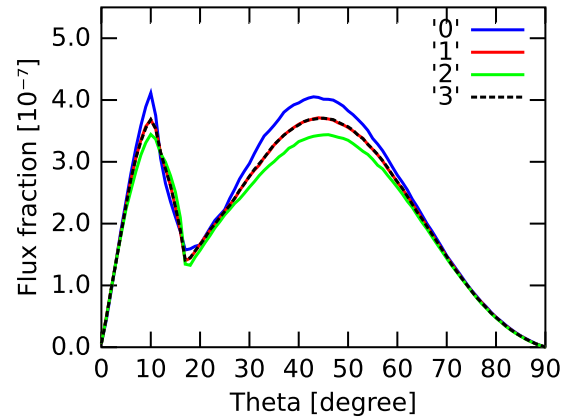


FIGURE 4. Calculated back-flux to four thruster channels with a total flux fraction of  $f = 8.0 \cdot 10^{-5}$ .

Thruster	$\int f(\theta) d\theta$
‘0’	$2.11 \cdot 10^{-5}$
‘1’	$2.00 \cdot 10^{-5}$
‘2’	$1.91 \cdot 10^{-5}$
‘3’	$2.00 \cdot 10^{-5}$

TABLE 1. Calculated back-flux to four thruster channels with a total flux fraction of  $f = 8.0 \cdot 10^{-5}$ .

These structures are determined by the combination of the mean ion energy distribution of the emitted Xenon ions, the sputter yield and the cosine distribution of the sputtered particles. The first peak at  $10^\circ$  is dominated by the maximum of the mean ion energy which takes place at the same emitting angle. The second peak is given by the combination of decreasing mean ion energy, with increasing  $\theta$  and increasing back-flow as given by the cosine law. For zero degree emission angle less flux is seen, due to the small number of emitted particles in this angular region, because of its small circular area for  $\theta \in [0; 1^\circ]$ .

For the ‘end-to-end’ simulations the same vacuum chamber was taken as a reference. A sketch of the implemented geometry is shown in Fig. 3. In order to reduce the artifacts further, all thrusters are pointing

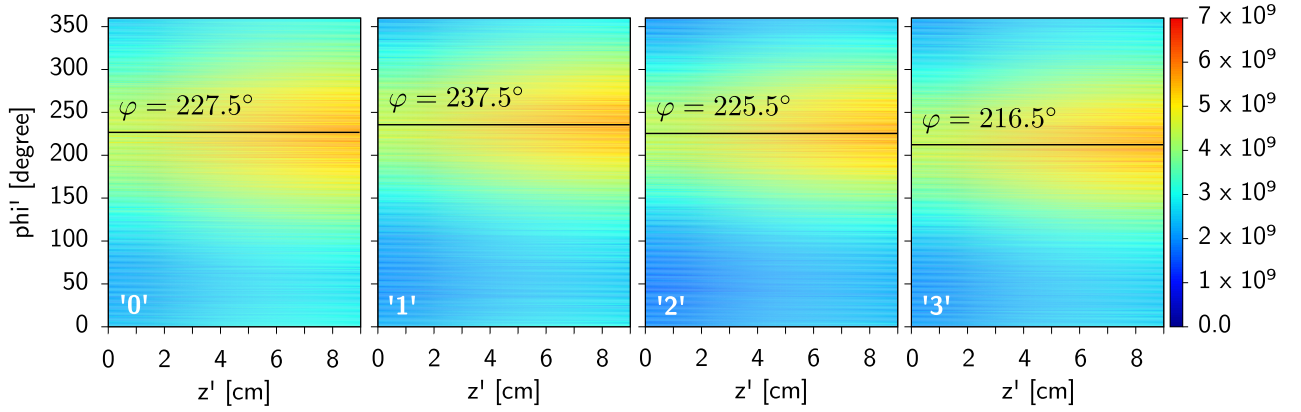


FIGURE 5. Re-deposited flux in  $\text{s}^{-1}\text{m}^{-2}$  inside the four 9 cm long thruster channels within an end-to-end test setup at the LVTF-1 vessel. Total re-deposited flux  $\Gamma = 4.3 \cdot 10^{+12} \text{m}^{-2}\text{s}^{-1}$

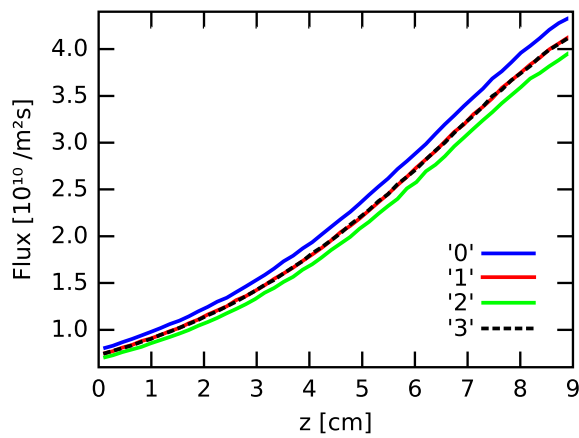


FIGURE 6. Re-deposited flux along the four thruster channels.

in the same direction. Thruster ‘0’ was chosen as the operating thruster.

The computed back-flux fractions towards the thruster exit planes of all four thrusters are shown in Fig. 4. The integral flux fraction for each thruster is given in Table 1. Most of the back-flux is measured for thruster ‘0’, since it is the emitting source. One can see that the integral deposited flux decreases with distance to the source. Therefore, equal flux distribution for symmetrically placed thrusters ‘1’ and ‘3’ is reasonable. Since the emitting source is not placed co-axially in the vessel one cannot deduce, where the sputtered particles originate from. In addition, the back-flux is no longer equally distributed in poloidal direction. In Fig. 5, the back-flux on the simplified inner thruster channel wall is given with respect to the depth  $z'$  and the poloidal angle  $\varphi$  of the thruster. Here the  $z'$ -axis is the symmetry axis of the cylinder, where  $z' = 0 \text{ cm}$  is at the anode and  $z' = 9 \text{ cm}$  is at the thruster exit. As expected, the flux is slightly higher in the thruster exit region and decreases towards the thruster bottom, see Fig. 6. It shows the measured flux summed over the poloidal angle. In poloidal di-

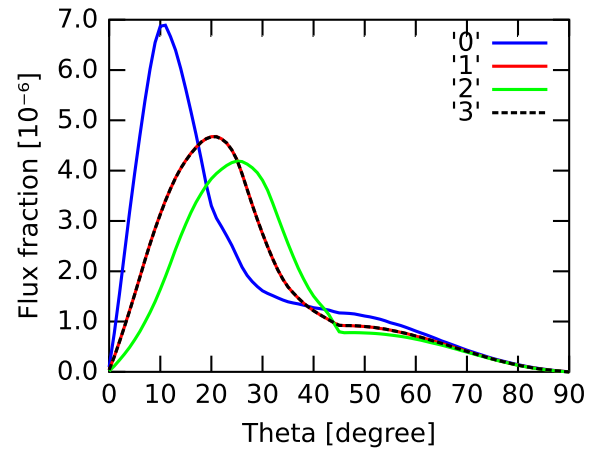


FIGURE 7. Calculated back-flux to four thruster channels with total flux fraction of  $f = 5.7 \cdot 10^{-4}$  at the ULAN vessel.

Thruster	$\int f(\theta) d\theta$
‘0’	$1.61 \cdot 10^{-4}$
‘1’	$1.42 \cdot 10^{-4}$
‘2’	$1.26 \cdot 10^{-4}$
‘3’	$1.42 \cdot 10^{-4}$

TABLE 2. Calculated back-flux to four thruster channels with total flux fraction of  $f = 5.7 \cdot 10^{-4}$  at the ULAN vessel.

rection, the distribution varies and the angle with maximum flux

$$\varphi = \max_{\varphi} \int n(\varphi, z') dz'$$

along the  $z$ -axis is given in each plot. Thrusters ‘0’ and ‘2’ show approximately the same maximum angle, while for the others the angle is shifted by  $\pm 10^\circ$ . This can be explained by the symmetric thruster positions within the vessel with respect to the emitting source. In total, the re-deposition distribution pattern is nearly the same for all four thrusters, due to the

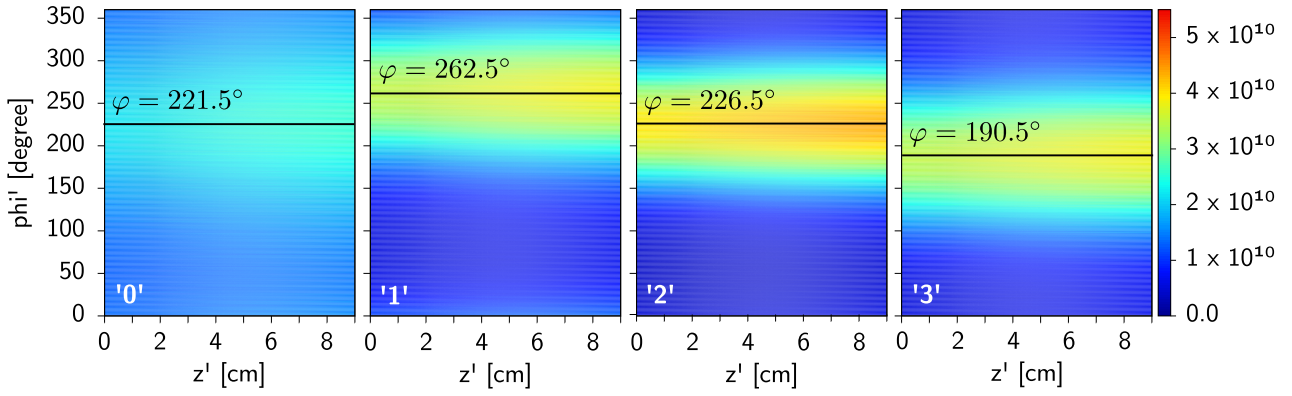


FIGURE 8. Re-deposited flux in  $\text{s}^{-1}\text{m}^{-2}$  inside the four 9 cm long thruster channels within an end-to-end test setup at the ULAN vessel. Total re-deposited flux  $\Gamma = 2.4 \cdot 10^{+13} \text{m}^{-2}\text{s}^{-1}$

large vessel geometry in comparison with the thruster size, and the narrow beam-like emission distribution.

For the purposes of comparison, the same simulation was carried out for a smaller vessel. The ULAN facility [14] in Ulm was modeled. It has a cylinder length of  $Z_c = 2.9 \text{m}$  and a radius of  $R_c = 1.2 \text{m}$ . As in Aerospazio, the thruster cluster is placed co-axially in the vessel. In Fig. 7, the back-flux fraction at the exit planes and the integral flux fraction are given in Table 2. The total back-flux fraction  $f = 5.7 \cdot 10^{-4}$  is about 14 times higher than for the larger Aerospazio vessel  $f = 8.0 \cdot 10^{-5}$ . A clearer distinction between the four thrusters and a different back-flux pattern develop. The maximum back-flux is measured for the emitting thruster '0', while it decreases with distance from the source, as can be seen in Tab. 2. These differences can be explained by the thruster position closer to the cylinder walls of the vessel. The back-flux for each channel is given in Fig. 8. Here, too, the re-deposition decreases with channel depth, as expected, but more pronounced re-deposition areas with parts of practically no re-deposition build up. In comparison with the larger vessel, the maximum peak is approximately one order higher. While for thruster '0' the re-deposition is almost equally distributed within the channel, a peak builds up with increasing distance from the emitting source, resulting in the highest maximum flux for thruster '2'. Also, the position of the maximum back-flux varies more in poloidal angles  $\varphi$ . Here, the symmetric thruster positions within the vessel with respect to the emitting source is important. These distribution characteristics correspond to observations during testing of the HEMP-T (B.van Reijen, personal communication, June, 2014).

Summarizing these results, a complex re-deposition profile appears due to the non-central position of the source within the vessel. Therefore, the source particles do not hit the vessel walls equally distributed in  $\varphi$ , which destroys the poloidal symmetry of the emitted flux hitting the vessel walls. In addition, the distribution of the sputtered particles is overlying, which gives no poloidal symmetry of the re-deposited particles, although the test-setup has such a simple

geometry. The size of the vessel not only influences the amount of re-deposited particles but also gives a more pronounced re-deposition pattern.

## 6. CONCLUSION

A Monte Carlo model using a ray approximation for the particles allows us to calculate the back-flux towards the thruster exit generated by sputtered particles at the vessel walls. It has shown the influence of the test set-up and the vessel size, which affects the re-deposition pattern inside the thruster channels. A non-centered emitting source leads to a complex re-deposition profile within the thruster channels. This effect can be diminished with a larger vacuum vessel which reduces the back-flux and smoothes the re-deposition patterns inside the channel. The emission distribution of the thruster itself also plays an important role. The results represent a worst case scenario, since the emission distribution of the thruster was assumed to be beam-like and aluminum was taken as the vessel wall material. For broader emission distributions and back-flux reducing modifications, e.g., carbon walls or baffles [2], the effects are reduced.

Effects like secondary electron emission at the vessel walls, which influence the plume potential, collisions of propellant ions with residual gas, regions of magnetized electrons in the plume and changes in the thruster potential due to re-deposited layers inside the channel are not considered within this model. In a future modeling step, the estimated back-flux distribution can be used for simulating the erosion and re-deposition on the thruster surfaces. This could clarify more precisely how terrestrial conditions influence the thrust measurements in total.

## ACKNOWLEDGEMENTS

This work was supported by the German Space Agency DLR through Project 50 RS 1101.

## REFERENCES

- [1] N. Koch, H.-P. Harmann, G. Kornfeld (eds.). *Status of the THALES High Efficiency Multi Stage Plasma Thruster Development for HEMP-T 3050 and HEMP-T*

- 30250, IEPC-2007-110. 30th International Electric Propulsion Conference, 2007.
- [2] O. Kalentev, K. Matyash, J. Duras, et al. Electrostatic Ion Thrusters - Towards Predictive Modeling. *Contributions to Plasma Physics* **54**:235–248, 2014. DOI:10.1002/ctpp.201300038.
- [3] K. Matyash, R. Schneider, A. Mutzke, et al. Kinetic Simulations of SPT and HEMP Thrusters Including the Near-Field Plume Region. *IEEE Transactions on Plasma Science* **38**(9, Part 1):2274–2280, 2010. DOI:10.1109/TPS.2010.2056936.
- [4] A. Genovese, A. Lazurenko, N. Koch, et al. (eds.). *Endurance Testing of HEMPT-based Ion Propulsion Modules for SmallGEO*, IEPC-2011-141. 32th International Electric Propulsion Conference, 2011.
- [5] R. Shastry, D. A. Herman, G. C. Soulas, M. J. Patterson (eds.). *Status of NASA's Evolutionary Xenon Thruster (NEXT) Long-Duration Test as of 50,000 h and 900 kg Throughput*, IEPC-2013-121. 33th International Electric Propulsion Conference, 2013.
- [6] R. Behrisch, W. Eckstein. Springer-Verlag.
- [7] V. Serikov, K. Nanbu. Monte Carlo numerical analysis of target erosion and film growth in a three-dimensional sputtering chamber. *Journal of Vacuum Science & Technology A: Vacuum, Surfaces, and Films* **14**(6):3108–3123, 1996. DOI:10.1116/1.580179.
- [8] C. Shon, J. Lee. Modeling of magnetron sputtering plasmas. *Applied Surface Science* **192**(1–4):258–269, 2002. Advance in Low Temperature RF Plasmas, DOI:10.1016/S0169-4332(02)00030-2.
- [9] L. King. *Transport-property and mass spectral measurements in the plasma exhaust plume of a Hall-effect space propulsion system*. Ph.D. thesis, University of Michigan, 1998.
- [10] A. Rai, A. Mutzke, R. Schneider. Modeling of chemical erosion of graphite due to hydrogen by inclusion of chemical reactions in SDTrimSP. *Nuclear Inst and Methods in Physics Research, B* **268**(17–18):2639–2648, 2010. DOI:10.1016/j.nimb.2010.06.040.
- [11] W. Eckstein. *Computer Simulation of Ion-Solid Interaction*, vol. 10 of *Springer Series in Material Science*. Springer, 1991.
- [12] O. Kalentev, L. Lewerentz, J. Duras, et al. Infinitesimal Analytical Approach for the Backscattering Problem. *Journal of Propulsion and Power* **29**(2):495–498, 2013. DOI:10.1002/ctpp.201300038.
- [13] AEROSPAZIO Tecnologie s.r.l. <http://www.aerospazio.com> [2014-02-01].
- [14] H.-P. Harmann, N. Koch, G. Kornfeld (eds.). *The ULAN Test Station and its Diagnostic Package for Thruster Characterization*, IEPC-2007-119. 30th International Electric Propulsion Conference, 2007.